Photo-Activated In Situ Supramolecular Reversible Self-Assembly Based on Amphiphilic Calix[4]arene for Information Encryption

Rong Zhang, Yong Chen, Lei Chen, Yi Zhang, and Yu Liu*

Photoacid sulfonato-merocyanine (MEH) serving as a photoisomer is added in mixed solution of amphiphilic calix[4]arene (SC4A8) and tetra-(4-pyridylphenyl) ethylene (TPE-4Py), which not only activates the in situ supramolecular self-assembly or disassembly, but also regulates two kinds of fluorescence emission. Benefiting from that MEH releases protons and becomes a ring-closed isomer spiropyran (SP) under 420 nm irradiation, TPE-4Py is protonated and then assembled with SC4A8 to form a supramolecular assembly with yellow fluorescence at 540 nm via electrostatic interactions. In the dark, SP changes to ring-opened MEH, realizing a spontaneous disassembly accompanied by fluorescence emission at 495 nm, and thus, a photo-activated reversible in situ supramolecular system is obtained successfully. Furthermore, Rhodamine B (RhB) acting as an energy acceptor is doped in the ternary supramolecular assembly, enabling the efficient energy transfer by the light irradiation. The formed tunable multicolor supramolecular assemblies have been successfully applied to the information encryption by 3D color codes.

1. Introduction

Stimulus-responsive luminescent materials have been paid considerable attention thanks to their tunable multicolor luminescence properties and potential applications in information encryption,[1] bioimaging/sensing,[2] and diagnosis.[3] In particular, photo-regulated luminescence materials are of great interest thanks to their non-invasive, good biocompatibility, controllable time, intensity, space, and high spatio-temporal resolution, which have been developed with much effort.[4] Compared with the conventional strategy for constructing such smart materials, which requires complex covalent modification of photosensitive fluorophores,[5] the supramolecular assembly

strategy can integrate functional molecules into the photo-responsive platform through non-covalent interaction forces, such as electrostatic interactions, hydrophobic interactions, host–guest interactions and so on, thus it is considered as one of the ideal ways to build smart materials.[6] Most reported photo-controlled supramolecular systems utilize photoresponsive molecules as both responsive and functional motifs. Recently, it is also an important issue to utilize photo-switchable platforms to load non-photoresponsive functional molecules to expand their application.[7] Zhao and co-workers reported a supramolecular system with photo-switch properties, which consisted of diarylethene and lanthanide coordination polymer between Eu^{3+} and bridged bis-2,6-pyridinedicarboxylic acid ligand, in which the isomerism of diaryl ethylene under UV and visible light irradiation was utilized, thus enabling the switched luminescence of lanthanide coordination polymer.[8] Kim and co-workers constructed photoswitchable self-assembly particles of amphiphilic spiropyran with reversible shape, color, and weak fluorescence upon UV and visible light irradiation.[9] Our group recently reported multicomponent supramolecular lanthanide photoswitch composed of azobenzene-bearing pyridinedicarboxylic acid, lanthanide ions, and the α-cyclodextrin, which utilized the entry or escape of azobenzene in α-cyclodextrin cavity due to the photoinduced conformational changes to realize photoswitchable luminescence function of lanthanide complexes.[10]

Among various hosts as building blocks of supramolecular assemblies, amphiphilic macrocycles have received extensive attention,[11] which construct multivalent co-assemblies through various non-covalent forces including electrostatic interactions as well as hydrophobic interactions and endow assemblies with unique functions.[12] However, the research on amphiphilic macrocycles as core structural motifs to integrate diverse photo-responsive components and functional units to construct multicomponent supramolecular assemblies and apply them to photo-controlled luminescent material is not sufficient. By constructing such a supramolecular system, photo-responsive components and functional modules can be combined closely without affecting their respective performance, and the function of the latter can be further regulated by

R. Zhang, Y. Chen, L. Chen, Y. Zhang, Y. Liu
College of Chemistry
State Key Laboratory of Elemento-Organic Chemistry
Nankai University
Tianjin 300071, P. R. China
E-mail: yuliu@nankai.edu.cn
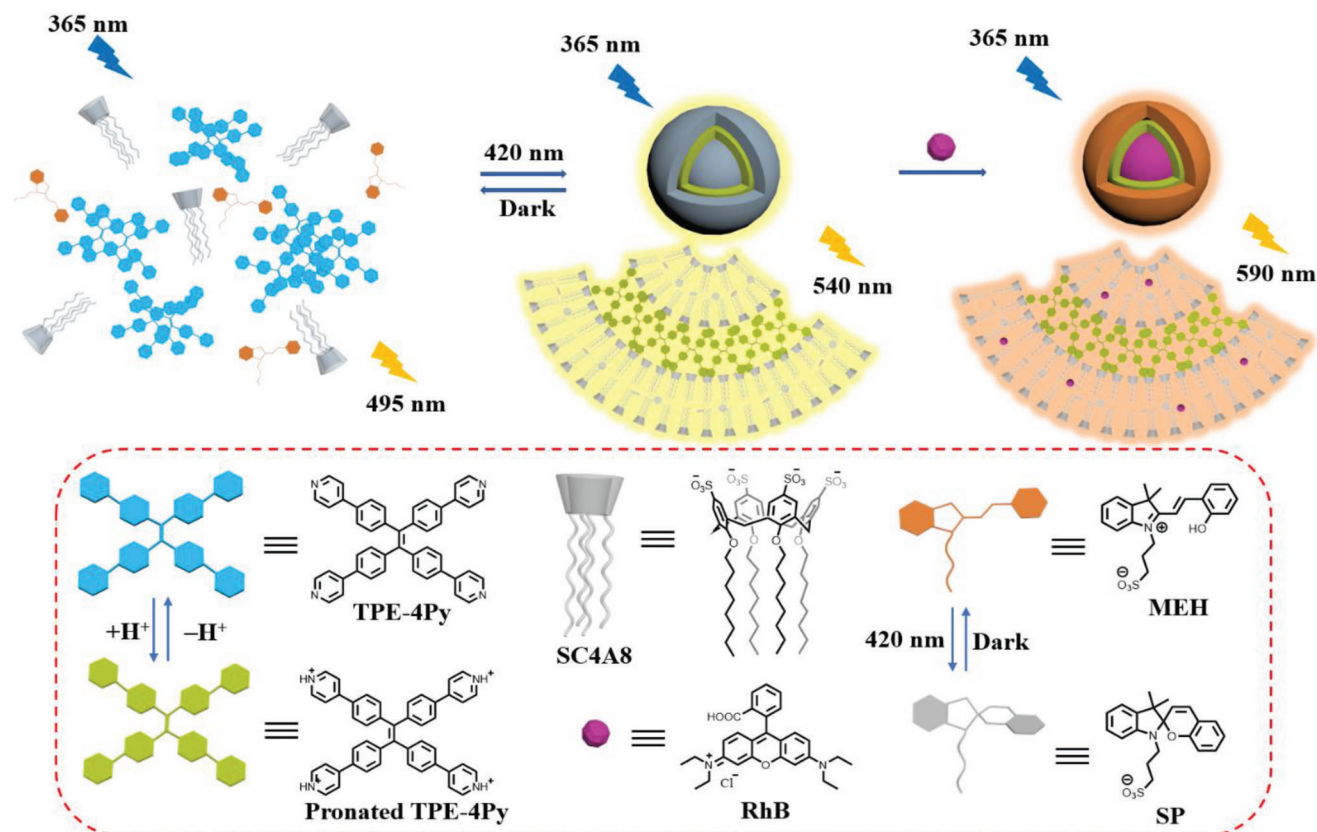
Scheme 1. Schematic illustration of constructing photo-activated multicomponent supramolecular assembly SC4A8/TPE-4Py/SP.

photoinduced changes of the former.[13] Herein, we constructed a photo-activated supramolecular assembly system based on amphiphilic calixarene (SC4A8), tetra-(4-pyridylphenyl) ethylene (TPE-4Py) and photoacid sulfonato-merocyanine (MEH). Due to the ability of photoacid to reversibly release and receive protons, which was different from other organic and inorganic acids,[14] and the pH-sensitive luminescence of TPE-4Py,[15] the multicolor luminescence function upon blue light irradiation was achieved by the effective assembly of TPE-4Py with MEH through the amphiphilic macrocyclic SC4A8, and the assembly was successfully applied to dynamic information encryption (**Scheme 1**). The positively charged TPE-4Py is obtained by the proton transfer path from ring-closed isomer spiropyran (SP) upon 420 nm irradiation and was subsequently assembled with the negatively charged SC4A8 to form a supramolecular assembly through electrostatic interactions. At the same time, MEH became the SP after irradiation and was loaded in the hydrophobic region of the assembly, accompanied by the fluorescence emission that gradually turned from blue to yellow. Subsequently, the fluorescence emission spontaneously returned to its original state after the light source was removed. Moreover, Rhodamine B (RhB) as an energy acceptor was doped into the SC4A8/TPE-4Py/SP assembly to produce an efficient energy transfer process. The supramolecular assembly strategy closely associates the acid-base response with the light response, endowing the originally pH-responsive system with light-controlled performance. Importantly, the photo-activated assembly process with the advantage

of real-time response was reversible, which was beneficial for the regulation of the assemblies and can be recycled for further applications. Therefore, the multi-component supramolecular assemblies could be successfully applied to dynamic information encryption via 3D encoding.

2. Results and Discussion

Owing to the potential of SC4A8 to efficiently assemble with protonated TPE-4Py through electrostatic interactions, their assembly behavior was characterized. In order to gain the optimal aggregation concentration between TPE-4Py and SC4A8, the critical aggregation concentration (CAC) test in the acetic acid buffer solution (pH 3.2) was carried out. In the presence of TPE-4Py, the transmittance at 550 nm decreased gradually with the increased concentration of SC4A8, indicating the important role of SC4A8 in inducing TPE-4Py aggregation. The inflection point of transmittance change was observed when the SC4A8 concentration was 4.4 µM (**Figure 1**a,b). Therefore, the CAC concentration of SC4A8 was measured as 4.4 µM in the TPE-4Py solution. Moreover, with the gradual addition of TPE-4Py to SC4A8 solution, the optical transmittance at 550 nm decreased slowly and then recovered gradually with an inflection point at 9 µM of TPE-4Py (Figure S1a,b, Supporting Information). The progressive decrease of the optical transmittance in the first stage suggested that TPE-4Py and SC4A8 formed a large assembly. As the concentration of TPE-4Py increased to an excessive amount,
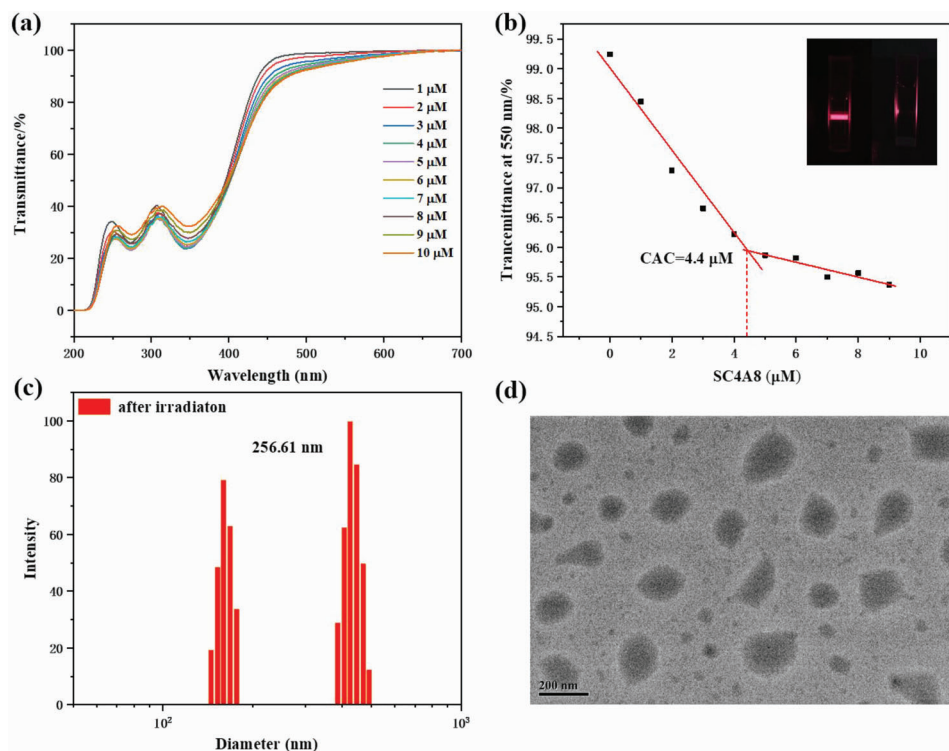
**ADVANCED
SCIENCE NEWS**

www.advancedsciencenews.com

**ADVANCED
OPTICAL
MATERIALS**

www.advopticalmat.de

Figure 1. a) Optical transmittance of SC4A8 with TPE-4Py versus the concentration of SC4A8 aqueous solution ([TPE-4Py] = 9 μм). b) Optical transmittance at 550 nm dependent on SC4A8 concentration. Inset photograph of the Tyndall effect of SC4A8/TPE-4Py/SP before and after irradiation. ([TPE-4Py] = 9 μм). c) Dynamic light scattering results and d) TEM images of SC4A8/TPE-4Py/SP after irradiation ([TPE-4Py] = 9 μм, [SC4A8] = 4.5 μм, [SP] = 90 μм).

the transmittance recovered instead caused by the dissociation of this simple complex. The change in transmittance conformed to the characteristics of the assembly formed by electrostatic interactions. Therefore, the optimal ratio of protonated TPE-4Py and SC4A8 to form assemblies was determined as 2:1 based on the CAC experimental results. A distinct Tyndall phenomenon was observed meanwhile, which could also demonstrate the formation of supramolecular assemblies (Figure 1b (inset)). The photophysical properties of MEH as a light-responsive unit were also investigated. The photoisomerization of photoacid MEH under light irradiation was tracked by changes of characteristic absorption peaks in UV–vis absorption spectroscopy. The absorption maximum at 424 nm (in order to observe the isomerization of MEN and SP, we mainly focus on observing the maximum absorption peak at 424 nm and the used concentration was low) gradually decreased after 420 nm irradiation for 30 s with the solution color changing from yellow to colorless (Figure S2a, Supporting Information), indicating that the ring-opened isomer MEH gradually changed into the ring-closed isomer SP under blue light irradiation. Then the characteristic absorption peak of MEH at 424 nm gradually recovered after the solution was placed in the dark for 10 min (Figure S2b, Supporting Information), suggesting a reversed isomerization from SP to MEH. In addition, the pH dropped during the conversion of MEH to SP due to the protons produced by the isomerization transition. Subsequently, the pH value recovered spontaneously in dark, reflecting the capacity of the photoacid MEH to reversibly release and acquire protons to regulate pH (Figure S3, Supporting Information).

Then, the photoacid MEH was introduced instead of the acetic acid buffer system to obtain light-responsive assemblies, and the photoinduced proton transfer process in the SC4A8/TPE-4Py/SP assembly was studied. To obtain the best ratio to promote the protonation of TPE-4Py, the absorption transformation of the assembly with the change of the photoacid concentration was investigated by UV absorption spectra and we reduced the concentration of each component in proportion to better observe the change of UV absorption. Since the characteristic absorption peaks of TPE-4Py and SP were close, the absorption peaks of the mixed solution were generally wide at 275−310 nm (λ_1) and 325−450 nm (λ_2) (Figure S4b, Supporting Information). Upon continuous 420 nm irradiation, λ_1 gradually increased as the concentration of SP increased, which was attributed to the absorption of TPE-4Py at 275 nm and the absorption of SP at 290 nm. Meanwhile, λ_2 composed of the absorption of TPE-4Py at 350 nm and the absorption of SP at 424 nm also increased. When SP increased to 9 times the equivalent of TPE-4Py, the absorption peak at 350 nm reached a stable state and changed no longer, indicating the protonation of TPE-4Py by SP. This was further confirmed in Figure S4c (Supporting Information) (which was obtained by subtracting Figure S4d, Supporting Information from Figure S4b, Supporting Information to show the characteristic absorption peak change of TPE-4Py protonated by SP), which was consistent with the absorption spectra of protonated TPE-4Py by acetic acid instead of photoacid (Figure S5, Supporting Information). These results indicated that the photoacid can effectively protonate TPE-4Py and the optimal ratio was 9 times the equivalent of TPE-4Py,
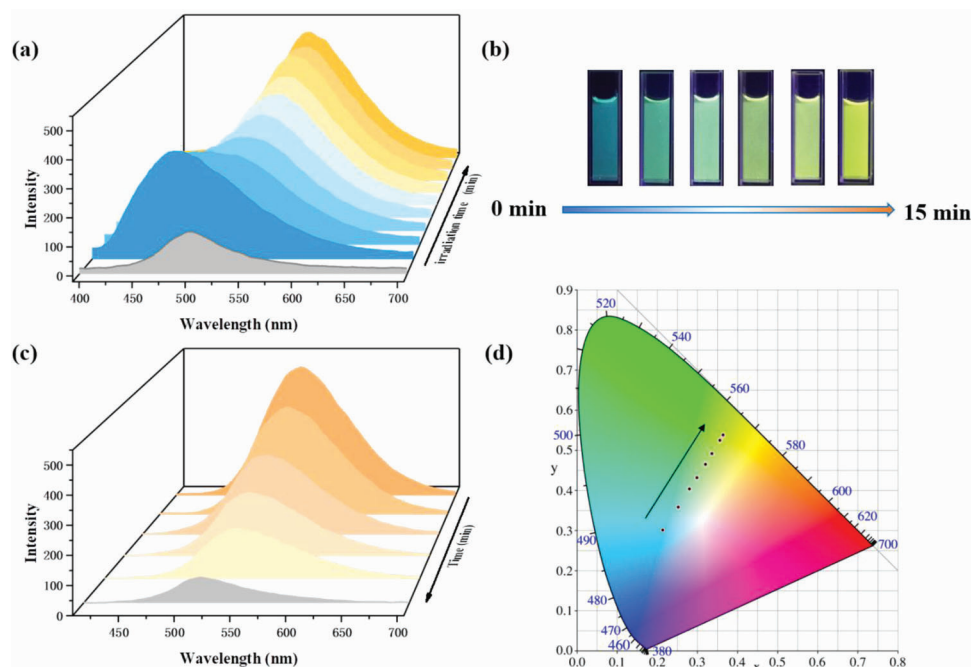
**ADVANCED
SCIENCE NEWS**

www.advancedsciencenews.com

**ADVANCED
OPTICAL
MATERIALS**

www.advopticalmat.de

Figure 2. a) Fluorescence spectra of SC4A8/TPE-4Py/SP upon 420 nm irradiation. b) Luminescence photograph of SC4A8/TPE-4Py/SP with 420 nm irradiation. c) Fluorescence spectra of SC4A8/TPE-4Py/SP after keeping in the dark. d) The CIE chromaticity diagram of the fluorescence color change of SC4A8/TPE-4Py/SP with continuous 420 nm irradiation ([TPE-4Py] = 9 μm, [SC4A8] = 4.5 μm, [SP] = 90 μm).

although it was less efficient to protonate TPE-4Py than acetic acid. To illustrate the formation of three-component assemblies under the activation of the blue light, we tested the changes in transmittance. As shown in Figure S6 (Supporting Information), the transmittance of the assemblies decreased. Moreover, we took the commonly used dialysis method for two days to separate the components that were not assembled, thereby the large assemblies were retained, which were evaluated by UV absorption spectrum, confirming the presence of three components in the assemblies (Figure S6, Supporting Information). Moreover, dynamic light scattering (DLS), and zeta electrical potential of the SC4A8/TPE-4Py/SP solution before and after irradiation was explored. The average hydrodynamic particle size of supramolecular assemblies increased according to the DLS results at the same time (Figure 1c and Figure S7, Supporting Information), confirming that the assemblies can only be formed in the presence of SC4A8, TPE-4Py, and SP. Moreover, the change in zeta electrical potential from −15.4 to −50.6 mV (Figure S8, Supporting Information) suggested the light-induced assembly led to a change in charge distribution. Furthermore, transmission electron microscopy (TEM) and scanning electron microscopy (SEM) measurements were taken to characterize the change in morphology and particle size of the SC4A8/TPE-4Py/SP assemblies. It was observed that the size of nanoparticles became larger after 420 nm irradiation with an average particle size of about 200 nm in the TEM images (Figure 1d and Figure S9, Supporting Information), indicating the assemblies formed nanoparticles, and similar morphology could be observed in SEM images (Figure S10, Supporting Information).

Subsequently, the spontaneous disassembly of the SC4A8/-TPE-4Py/SP supramolecular assembly after the removal of the

light source was further investigated. When the assembly was left in dark, the color of the solution slowly recovered from colorless to the original yellow. After 2 h, the solution color no longer changed, and the UV absorbance was also recovered to the original state (Figure S11a, Supporting Information), indicating the feasibility of the disassembly. The transformation of the absorbance between the dispersed solution and the SC4A8/TPE-4Py/SP nanoparticles could be reversibly transformed at least 5 times without significant attenuation (Figure S11b, Supporting Information). The reversible conversion was also reflected in the value of pH. With the assembly and disassembly of SC4A8/TPE-4Py/SP, the change of pH could also be cycled more than 5 times (Figure S3, Supporting Information), suggesting the reversible regulation of pH changes in assemblies by photoacid.

In order to explore the two different fluorescence emission behaviors excited at the same wavelength of the SC4A8/TPE-4Py/SP supramolecular assembly before and after irradiation, the photo-responsive properties were investigated by fluorescence spectroscopy. Initially, SC4A8/TPE-4Py/SP exhibited a weak emission peak at 495 nm. Upon irradiation at 420 nm for 10 s, a significantly enhanced fluorescence at 475 nm was immediately observed which was derived from the partial aggregation of TPE-4Py in neutral aqueous solution, and then its intensity gradually decreased accompanied by the appearance of a new fluorescence emission at 540 nm following the extension of the irradiation time (**Figure 2**a). After 15 min of irradiation, the fluorescence emission reached photostability, and the intensity was finally enhanced by 5 times compared to the initial value. The blue-to-yellow luminescent color was also observed both in an aqueous solution (Figure 2b and Movie S1, Supporting

**ADVANCED
SCIENCE NEWS**

www.advancedsciencenews.com

**ADVANCED
OPTICAL
MATERIALS**

www.advopticalmat.de

Information) and hydrogel (Figure S12, Supporting Information). The real-time fluorescence changes demonstrated that the assembly formation of SC4A8/TPE-4Py/SP. The fluorescence color coordinates were depicted in the CIE chromaticity diagram by calculation, which showed the same color change (Figure 2d). The luminescent transition might be explained by the fact that the ring-opened MEH partially quenched the fluorescence through the energy transfer,[16] while the ring-closed state induced by the blue light irradiation no longer quenched the luminescence, thus the TPE-4Py rapidly restored its original blue luminescence due to the partial aggregation in aqueous solution. With continuous irradiation, the solution pH gradually dropped, enhancing the acidity and increasing the protonation of TPE-4Py and red-shifting the fluorescence emission. Meanwhile, the negatively charged SC4A8 aggregated the protonated TPE-4Py through electrostatic interactions, thereby the luminescence intensity was significantly enhanced. Additionally, as the fluorescence intensity of the SC4A8/TPE-4Py/SP supramolecular assembly was significantly enhanced after irradiation, the quantum yield was also increased from 13.98% to 24.82% (Figure S13, Supporting Information). Moreover, the importance of electrostatic interactions for assembling with TPE-4Py was demonstrated by comparing different negatively charged macrocyclic hosts. It was found that both SC4A8 and sulfobutylether-β-cyclodextrin (SBE-β-CD) led to the redshift and the enhancement of fluorescence (Figure S14, Supporting Information). In comparative experiments, the photoacid was replaced by acetic acid to protonate TPE-4Py, which exhibited similar fluorescence enhancement at 540 nm after gradually increasing the concentration of SC4A8 (Figure S15, Supporting Information). Furthermore, we tested the fluorescence spectra of TPE-4Py and SC4A8/TPE-4Py systems at different pH (Figure S16, Supporting Information). TPE-4Py partially aggregated in neutral aqueous solution and emitted fluorescence at 475 nm, then the fluorescence emission gradually transitioned from 475 to 540 nm with the decrease of pH. This demonstrated that the yellow luminescence of the supramolecular assembly after irradiation derived from the redshift of protonated TPE-4Py in an acidic system. Additionally, the reversed luminescence transformation was also explored. After removing the external light source, the emission peak at 540 nm not only decreased slowly in intensity but also had a slight blue shift. After 2 h in dark, the fluorescence intensity no longer decreased, and the emission peak returned to the initial state at 495 nm (Figure 2c). The gradual decrease in fluorescence intensity of the assemblies under dark conditions could be explained by that the photoacid SP spontaneously changed to the ring-closed isomer in dark, which quenched the fluorescence emission due to energy transfer. The photocycle could be repeated 5 times without significant fatigue (Figure S17, Supporting Information). In the control experiment, the mixed solution of TPE-4Py and photoacid without SC4A8 exhibited a weak emission peak at 495 nm in dark, which was consistent with the luminescence in the presence of SC4A8. Then the fluorescence intensity gradually enhanced under continuous 420 nm irradiation, which reached a stable state after 15 min (Figure S18, Supporting Information). It was worth noting that the fluorescence red-shift of the system was not observed even if the irradiation time was extended to 40 min, revealing the indispensability of the host SC4A8 in regulating the luminescence of the assembly.

Considering the hydrophobic regions and the negatively charged surface of the SC4A8/TPE-4Py/SP assembly as well as its bright luminescence at 540 nm, we conjectured that it could be used as an energy donor for the controllable fluorescence resonance energy transfer (FRET). Thus, the FRET progress between supramolecular assemblies and dyes activated by the blue light was investigated. To further broaden the variation range of the fluorescence emission, RhB was selected as the energy acceptor since its UV absorption peak had a good overlap with the fluorescence emission peak of the SC4A8/TPE-4Py/SP assemblies at 540 nm after blue light irradiation (**Figure 3**a). As shown in Figure S19a (Supporting Information), with the addition of RhB to SC4A8/TPE-4Py/SP after irradiation, a gradual decrease in the characteristic emission peak at 540 nm of the assemblies was observed, a new emission peak at 590 nm appeared and gradually increased when excited at 365 nm. The calculated energy transfer efficiency was 65% when the ratio of donor/acceptor (D/A) was 5:1. In addition, fluorescence lifetime experiments revealed that the lifetimes of TPE-4Py/MEH and SC4A8/TPE-4Py/SP were 4.33 and 3.88 at 540 nm, respectively. While the lifetime at 540 nm was reduced to 2.98 ns after the introduction of RhB (Figure S20, Supporting Information). Additionally, no significant emission at 590 nm was observed for either RhB or RhB/TPE-4Py/MEH under the same conditions (Figure S21, Supporting Information). In control experiment, only SC4A8 was replaced with the same concentration of negatively charged calix[4]arene (SC4A) (lack of hydrophobic alkyl chain) which also enabled the aggregation of protonated TPE-4Py, however, the SC4A/TPE-4Py/SP/RhB mixed system did not occur FRET process from SC4A/TPE-4Py/SP to RhB (Figure S22, Supporting Information), indicating the variation of the fluorescence was attributed to the energy transfer from supramolecular assemblies to dyes. In addition, the green channel and the red channel of confocal fluorescence microscopic imaging were merged very well, indicating that the energy acceptor RhB was loaded in the assembly (Figure S22, Supporting Information). The efficient energy transfer between SC4A8/TPE-4Py/SP and RhB might be due to the fact that the hydrophobic region in the assemblies could load RhB, bringing the energy acceptor closer to the luminescence center of the donor to facilitate energy transfer. Furthermore, the response of the energy transfer performance to light was explored. Under the continuous 420 nm irradiation, it was also observed that the emission peak at 540 nm decreased followed by the orange fluorescence at 590 nm increased when the ratio of the energy acceptor was 1/5 of the donor (Figure 3b), in which the energy transfer efficiency was 45%. The transition of fluorescence color from yellow to orange was observed, which was also depicted in the CIE chromaticity diagram (Figure 3d). Subsequently, after turning off the 420 nm light source, the emission peak at 590 nm decreased slowly until it no longer attenuated after 2 h in dark (Figure 3c). These results suggested the supramolecular assembly was still responsive to the blue light even after the dye loading, resulting in the light-controlled energy transfer. Moreover, in order to expand the universality of supramolecular assembly as an energy donor, the energy transfer between SC4A8/TPE-4Py/SP and sulfonated rhodamine 101 (SR101) as well as Nile Blue (NiB) was also investigated. Gradually adding SR101 upon irradiation, the emission peak of assemblies decreased with the enhanced intensity of the emission peak
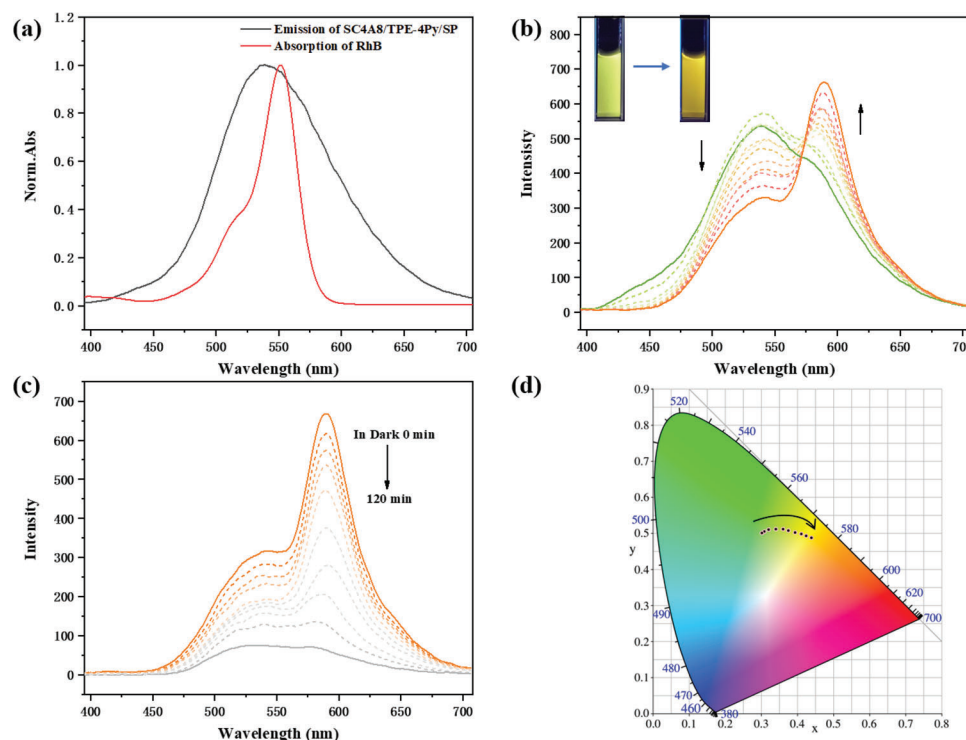
Figure 3. a) Normalized absorption spectra of RhB and emission spectra of SC4A8/TPE-4Py/SP. b) Fluorescence emission spectra of SC4A8/TPE-4Py/SP with 0.2 eq. RhB upon 420 nm irradiation (Inset: photographs of SC4A8/TPE-4Py/SP with RhB before and after 420 nm irradiation). c) Fluorescence emission spectra of SC4A8/TPE-4Py/SP/RhB complexes after removing the light source. d) The CIE chromaticity diagram of the color change of SC4A8/TPE-4Py/SP/RhB with continuous 420 nm irradiation ([TPE-4Py] = 9 μM, [SC4A8] = 4.5 μM, [SP] = 90 μM, [RhB] = 1.8 μM).

at 610 nm (Figure S19b, Supporting Information). Similarly, by increasing NiB, the original emission peak of the assembly decreased rapidly, and the fluorescence peak at 650 nm enhanced (Figure S19c, Supporting Information). The maximum energy transfer efficiency was 30% for the former when the ratio of D/A was 1:1, and the energy transfer efficiency of the latter reached the maximum value of 80% at the ratio of D/A for 8:1.

In view of the light-controlled multicolor luminescence properties of the assemblies, we applied them to the information encryption using 3D color codes, which utilized different color blocks (usually composed of blue, green and red) to form a colorful pattern, and then the information was read by software scanning.[17] To produce the encrypted patterns, the prepared assembly solution was poured into small square containers, and the solution of different components produced different fluorescence color changes upon the same blue light irradiation. The composition of the solutions emitting blue, yellowish green and orange fluorescence are TPE-4Py/SP, SC4A8/TPE-4Py/SP, SC4A8/TPE-4Py/SP/RhB respectively. The number and specific arrangement of colors generated distinct information that could be edited, interpreted and stored via a smartphone software APP COLORCODE. As shown in **Figure 4**a, the solution in the small boxes under sunlight was yellow, and there was no obvious difference in the luminescent color in each container under the 365 nm UV light. Therefore, no information can be obtained at this time. Upon 420 nm irradiation for 15 min, the fluorescence color changed so that code A could be obtained under UV lamp with a specific arrangement of three colors. The code was then

scanned to obtain the hidden information "NKU" with the help of the software (Movie S2, Supporting Information). Once the blue light exposure was removed, the fluorescence color slowly returned to the original state accompanied by the information hiding (Figure 4b). In addition, dynamic encoding was also achieved by adjusting the position of containers through a specific route. For example, after replacing the position, code A was converted into code B, thus the stored information changed from "NKU" to "C." Code B also responded to the 420 nm irradiation, enabling the information reading and encryption (Movie S3, Supporting Information). The dynamic transformation in coding could be reversible multiple times using irradiation and physical adjustments to the position of the small boxes. Additionally, the information could also be stored using a 96-well plate, which visually displayed the encrypted content under the UV light (Figure S23, Supporting Information).

3. Conclusion

In conclusion, the photo-activated in situ supramolecular assemblies with multicolor luminescence was successfully constructed by using SC4A8, TPE-4Py and photoacid MEH. Taking advantage of abundant negative charges and hydrophobic long chains of amphiphilic SC4A8, the photoacid isomer SP after irradiation was loaded in the hydrophobic region, and the photoacid-induced protonated TPE-4Py can assemble with SC4A8 through electrostatic interactions. The changes in fluorescence emissions were derived from the protonation of TPE-4Py, and the inverse
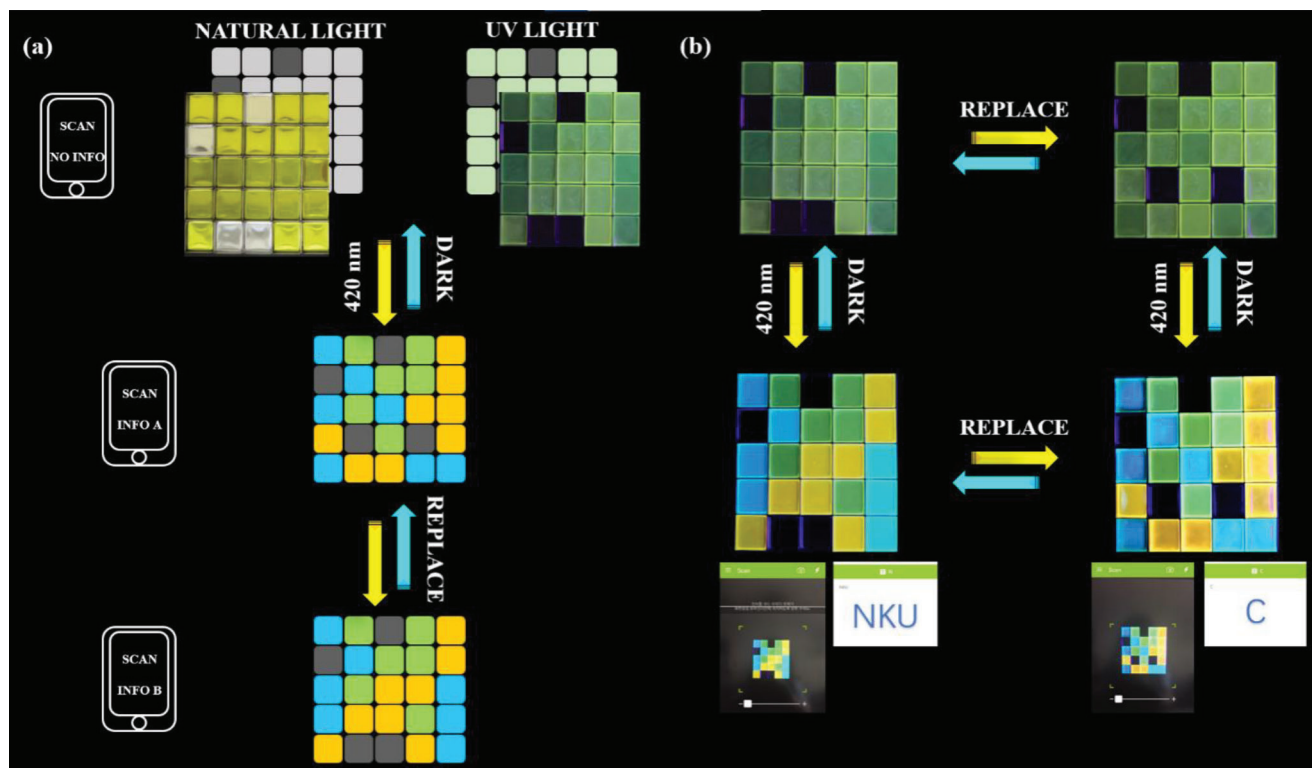
**ADVANCED
SCIENCE NEWS**

www.advancedsciencenews.com

**ADVANCED
OPTICAL
MATERIALS**

www.advopticalmat.de

Figure 4. a) Schematic illustration of the 3D code encryption. b) Photographs of photo-responsive 3D code transformation and corresponding information was read by smartphone software ([TPE-4Py] =9 µm, [SC4A8] = 4.5 µm, [SP] = 90 µm, [RhB] = 1.8 µm).

reaction was visualized due to the disassembly from SC4A8. Moreover, RhB was loaded in the SC4A8/TPE-4Py/SP assemblies, which achieved efficient energy transfer. Therefore, using photoacid MEH not only realized photo-activated in situ reversible supramolecular assemblies, but also regulated two different fluorescence emissions at 495 and 540 nm under the same excitation wavelength, and efficient energy transfer occurred between the fluorescence emission at 540 nm of assembly and RhB, which was successfully applied in 3D encoded information encryption.

Supporting Information

Supporting Information is available from the Wiley Online Library or from the author.

Acknowledgements

Conflict of Interest

The authors declare no conflict of interest.

Data Availability Statement

The data that support the findings of this study are available from the corresponding author upon reasonable request.

Keywords

[1] a) J. Zhang, B. Z. He, Y. B. Hu, P. Alam, H. K. Zhang, J. W. Y. Lam, B. Z. Tang, *Adv. Mater.* **2021**, *33*, 2008071; b) Y. Y. Wang, Y. M. Zhang, S. X. A. Zhang, *Acc. Chem. Res.* **2021**, *54*, 2216;. c) Y. Sun, X. X. Le, S. Y. Zhou, T. Chen, *Adv. Mater.* **2022**, *34*, 2201262; d) L. J. Ding, X. D. Wang, *J. Am. Chem. Soc.* **2020**, *142*, 13558.

[2] a) J. J. Chen, L. Q. Chen, Y. L. Wu, Y. C. Fang, F. Zeng, S. Z. Wu, Y. L. Zhao, *Nat. Commun.* **2021**, *12*, 6870;. b) Z. Li, X. F. Xia, Y. You, F. Y. Wang, C. F. Lu, G. C. Yang, C. Ma, J. Q. Nie, Q. Sun, S. L. Wu, J. Ren, *Chin. Chem. Lett.* **2021**, *32*, 1785.

[3] a) H. Feng, Z. Q. Zhang, Q. T. Meng, H. M. Jia, Y. Wang, R. Zhang, *Adv. Sci.* **2018**, *5*, 1800397; b) X. H. Wu, Y. X. Lu, B. Liu, Y. Chen, J. F. Zhang, Y. Zhou, *Chin. Chem. Lett.* **2021**, *32*, 2380.

[4] a) J. J. Zhang, Q. Zou, H. Tian, *Adv. Mater.* **2013**, *25*, 378;. b) Z. Q. Li, H. Z. Chen, B. Li, Y. M. Xie, X. L. Gong, X. Liu, H. R. Li, Y. L. Zhao, *Adv. Sci.* **2019**, *6*, 1901529; c) J. Volaric, W. Szymanski, N. A. Simeth,

**ADVANCED
SCIENCE NEWS**

www.advancedsciencenews.com

**ADVANCED
OPTICAL
MATERIALS**

www.advopticalmat.de

B. L. Feringa, *Chem. Soc. Rev.* **2021**, *50*, 12377;. d) J. Y. Zhang, H. C. Shen, X. Y. Liu, X. Q. Yang, S. L. Broman, H. R. Wang, Q. Y. Li, J. W. Y. Lam, H. K. Zhang, M. Cacciarini, M. B. Nielsen, B. Z. Tang, *Angew. Chem., Int. Ed.* **2022**, *61*, e202208460.

[5] Q. K. Qi, G. Sekhon, R. Chandradat, N. M. Ofodum, T. R. Shen, J. Scrimgeour, M. Joy, M. Wriedt, M. Jayathirtha, C. C. Darie, D. A. Shipp, X. G. Liu, X. C. Lu, *J. Am. Chem. Soc.* **2021**, *143*, 17337.

[6] a) T. L. Mako, J. M. Racicot, M. Levine, *Chem. Rev.* **2019**, *119*, 322;. b) L. Chen, Y. Chen, H. G. Fu, Y. Liu, *Adv. Sci.* **2020**, *7*, 2000803; c) X. Y. Lou, Y. W. Yang, *Adv. Mater.* **2020**, *32*, 2003263; d) Y. M. Zhang, Y. H. Liu, Y. Liu, *Adv. Mater.* **2020**, *32*, 806158; e) Y. Zhang, C. Zhang, Y. Chen, J. Yu, L. Chen, H. Zhang, X. F. Xu, Y. Liu, *Adv. Opt. Mater.* **2022**, *10*, 2102169. f) Z. Li, Z. Q. Yang, Y. A. Zhang, B. Yang, Y. W. Yang, *Angew. Chem., Int. Ed.* **2022**, *61*, e2022061; g) Z. Li, Y. W. Yang, *Acc. Mater. Res.* **2021**, *2*, 292. h) I. Yildiz, S. Impellizzeri, E. Deniz, B. McCaughan, J. F. Callan, F. M. Raymo, *J. Am. Chem. Soc.* **2011**, *133*, 871.

[7] X. X. Le, H. Shang, S. S. Wu, J. W. Zhang, M. J. Liu, Y. F. Zheng, T. Chen, *Adv. Funct. Mater.* **2021**, *31*, 2108365.

[8] Z. Q. Li, X. Liu, G. N. Wang, B. Li, H. Z. Chen, H. R. Li, Y. L. Zhao, *Nat. Commun.* **2021**, *12*, 1363.

[9] J. Kim, H. Yun, Y. J. Lee, J. Lee, S. H. Kim, K. H. Ku, B. J. Kim, *J. Am. Chem. Soc.* **2021**, *143*, 13333.

[10] H. J. Yu, H. R. Wang, F. F. Shen, F. Q. Li, Y. M. Zhang, X. F. Xu, Y. Liu, *Small* **2022**, *18*, 2201737.

[11] a) P. Y. Li, Y. Chen, C. H. Chen, Y. Liu, *Chem. Commun.* **2019**, *55*, 11790; b) X. M. Chen, K. W. Cao, H. K. Bisoyi, S. Zhang, N. N. Qian, L. X. Guo, D. S. Guo, H. Yang, Q. Li, *Small* **2022**, *18*, 2204360.

[12] a) Z. X. Liu, X. H. Sun, X. Y. Dai, J. J. Li, P. Y. Li, Y. Liu, *J. Mater. Chem.* **2021**, *9*, 1958; b) H. Wang, X. X. Xu, Y. C. Pan, Y. X. Yan, X. Y. Hu, R. W. Chen, B. J. Ravoo, D. S. Guo, T. Zhang, *Adv. Mater.* **2021**, *33*, 2006483.

[13] a) X. M. Chen, X. F. Hou, H. K. Bisoyi, W. J. Feng, Q. Cao, S. Huang, H. Yang, D. Z. Chen, Q. Li, *Nat. Commun.* **2021**, *12*, 4993;. (b) X. M. Chen, W. J. Feng, H. K. Bisoyi, S. Zhang, X. Chen, H. Yang, Q. Li, *Nat. Commun.* **2022**, *13*, 3216.

[14] a) F. M. Raymo, S. Giordani, *J. Am. Chem. Soc.* **2001**, *123*, 4651;. b) J. Guo, H. Y. Zhang, Y. Zhou, Y. Liu, *Chem. Commun.* **2017**, *53*, 6089; c) T. Zhang, L. Sheng, J. N. Liu, L. Ju, J. H. Li, Z. Du, W. R. Zhang, M. J. Li, S. X. A. Zhang, *Adv. Funct. Mater.* **2018**, *28*, 1705532.

[15] Z. Li, P. C. Liu, X. F. Ji, J. Y. Gong, Y. B. Hu, W. J. Wu, X. N. Wang, H. Q. Peng, R. T. K. Kwok, J. W. Y. Lam, J. Lu, B. Z. Tang, *Adv. Mater.* **2020**, *32*, 1906493.

[16] Z. Lin, H. Wang, M. L. Yu, X. Guo, C. H. Zhang, H. T. Deng, P. S. Zhang, S. Chen, R. J. Zeng, J. X. Cui, J. Chen, *J. Mater. Chem.* **2019**, *7*, 11515.

[17] Q. Wang, B. Y. Lin, M. Chen, C. X. Zhao, H. Tian, D. H. Qu, *Nat. Commun.* **2022**, *13*, 4185.